CrystEngComm

Structural evolution of amorphous calcium sulfate nanoparticles into crystalline gypsum phase

Journal:	*CrystEngComm*
Manuscript ID	CE-ART-08-2020-001173.R1
Article Type:	Paper
Date Submitted by the Author:	24-Aug-2020
Complete List of Authors:	Jia, Caiyun; Zhejiang university, Department of Environmental Engineering Wu, Luchao ; Zhejiang University, Environmental & Resource Sciences Chen, Qiaoshan; Zhejiang University, Department of Environmental Engineering Ke, Peng; Zhejiang University, Department of Environmental Engineering De Yoreo, James; PNNL, Materials Synthesis and Simulation Guan, Baohong; Zhejiang University, Department of Environmental Engineering

Structural evolution of amorphous calcium sulfate nanoparticles into crystalline gypsum phase

Caiyun Jia,[a,b] Luchao Wu,[a] Qiaoshan Chen,[a] Peng Ke,[a] James J. De Yoreo,[b, c] and Baohong Guan [a,d]*

[a]College of Environmental and Resource Sciences, Zhejiang University, Hangzhou 310058, China *E-mail: guanbaohong@zju.edu.cn; Tel +86 571-88982026; Fax +86 571-88982026

[b]Physical Science Division, Pacific Northwest National Laboratory, Richland, WA 99352, USA

[c]Department of Materials Science and Engineering, University of Washington, Seattle, WA 98195, USA

[d]Key Laboratory of Environment Remediation and Ecological Health, Ministry of Education, Hangzhou 310058, China

Electronic supplementary information (ESI) available. See DOI: 10.1039/xxx

ORCID

Baohong Guan: 0000-0001-6183-3979

James J. De Yoreo: 0000-0002-9194-6699

Abstract

The involvement of amorphous calcium sulfate (ACS) as a precursor to calcium sulfate crystallization remains an important but poorly understood phenomenon, especially the mechanism by which ACS evolves to the crystalline phase. Here we captured the ACS nanoparticles as a precursor to calcium sulfate crystallization in a concentrated $CaCl_2$ solution at 90 ^oC and observed several stages of its evolution. The ACS nanoparticles grew by simultaneous fusion and internal structural evolution. Aggregation of the ACS nanoparticles gave birth to the bulk ACS particle within which nanocrystalline domains sprout and developed into the crystalline gypsum. This work deepens the understanding of the evolution of ACS nanoparticles and its role in multistage crystallization of calcium sulfate.

Introduction

Crystallization is of considerable importance in the generation of materials and it is well accepted that many properties of an emerging solid phase have already been determined at the onset of crystallization.[1-4] A profound understanding of the crystallization process will contribute to controlling or regulating the progress of crystallization in certain desired directions.[5-7] In contrast to what has been described in the classical nucleation theory, the birth of crystals via multistage crystallization pathways is a hot topic in materials sciences and an increasing number of studies have observed the formation of amorphous precursors before crystallization of the solid phase.[8-12] As for the transformation of amorphous precursors to crystalline phase, the mechanism of solid-state transformation[13-16] as well as dissolution-reprecipitation[17-19] has been proposed. However less information is available on the details about the structural evolution within the amorphous precursors.

Calcium sulfate, as a naturally abundant and industrially important mineral with three distinct crystalline phases differing in the degree of hydration: gypsum ($CaSO_4 \cdot 2H_2O$), bassanite ($CaSO_4 \cdot 0.5H_2O$) and anhydrite ($CaSO_4$), has attracted much attention of the geologists and mineralogists.[20, 21] In the past few years, the laboratory synthesis of various calcium sulfate phases have provided a better understanding of its origin and behavior in natural environments as well as the basis of its applications in industry.[22-26] A growing body of evidence supports the notion of multistage processes governing the formation of gypsum from aqueous solutions at room temperature, and an amorphous calcium sulfate (ACS) precursor prior to the final

crystalline gypsum phase has been observed.[27-29] However, still much remains undiscovered concerning the role of ACS as a precursor to calcium sulfate crystallization and the mechanism by which the ACS precursor evolves to the crystalline phase.

Here in this work we tried to investigate the early stages of the crystallization pathway of calcium sulfate phases in a low calcium sulfate concentration so as to prolong the crystal nucleation rate and therefore to have enough time to obtain the amorphous precursors in the initial stages. The vacuum / solvent filtration sample quenching method and cryogenic sample quenching method, together with the high-resolution (cryo)-TEM (HRTEM) and low-dose selected area electron diffraction (SAED) techniques were applied to obtain the morphological and structural information.

Experimental section

Synthesis of calcium sulfate nanoparticles

The required analytical reagent grade $CaCl_2 \cdot 2H_2O$, Na_2SO_4 and ethanol were purchased from Sinopharm Chemical Reagent Co., Ltd., Shanghai, China. The precursor solutions of 3.00 M $CaCl_2$ and 50.00 mM Na_2SO_4 were prepared by dissolving the certain amounts of $CaCl_2 \cdot 2H_2O$ and Na_2SO_4 into certain volumes of deionized water. Since the dissolution of $CaCl_2 \cdot 2H_2O$ was exothermic, the 3.00 M $CaCl_2$ solution was dilute to certain volume until the solution temperature was cooled down to room temperature. Then the two precursor solutions were filtered with 0.22 μm membrane twice to remove the possible insoluble substances. The 0.22 μm membrane was

purchased from Shanghai Xingya purification material Factory, China. The batch experiments were performed in a 150 mL Teflon reactor with constant magnetic stirring at 90 ^{o}C (with a deviation of ± 0.5 ^{o}C). In a typical prodedure, 115.0 mL of $CaCl_2$ solution and 10.0 mL of Na_2SO_4 solution were preheated to 90 ^{o}C separately, and then the Na_2SO_4 solution was added into the $CaCl_2$ solution immediately to obtain the final calcium sulfate concentrations of 4.00 mM. At the selected time intervals (from 1 min to 40 min), 1.0 mL of solution was taken from the reactor and rapidly vacuum filtered onto the carbon coated Cu-TEM grids that were purchased from Beijing Zhongjing Keyi Instrument Technology Co. LTD, China, and then 1.0 mL of ethanol was added immediately to rinse the sample for removal of the possible residual ions.[23, 30] After that the grids were irradiated under the infrared lamp for seconds to vaporize the residual ethanol. The prepared samples were stored in a vacuum desiccator for use.

In order to demonstrate that the vacuum / solvent filtration sample quenching method does not affect the crystallization pathway, a cryogenic sample quenching method was applied using a fully automated vitrification robot (FEI Vitrobot Mark III) equipped with humidity and temperature controlled glove box.[13, 31-33] The cryo-TEM grids (R2/2 Quantifoil Jena Grids), which were 200 mesh copper grids covered by a carbon film that contained a regular pattern of 2 μm holes in the carbon layer, were purchased from the Quantifoil Micro Tools GmbH. After the surface plasma treatment using a Cressington 208 carbon coater, the grids were assembled in the automated vitrification robot prior to the vitrification procedure. After reaction for 1 min, small aliquots (3.0 μL) of solution was taken from the reactor and immediatly deposited onto the

cryo-TEM grids. The automated vitrification robot removed the excess liquid and produced a thin liquid layer of around 100 nm thick containing the calcium sulfate nanoparticles. Thereafter, the cryo-TEM grids were plunged into the liquid ethane which was prior cooled down by the liquid nitrogen to ~ -170 ^{o}C. The frozen cryo-TEM grids were re-equilibrated in a liquid nitrogen dewar for use.

Sample characterization

The samples were subjected to the high-resolution transmission electron microscopy (HRTEM) using a Tecnai G2 F20 S-TWIN field emission gun microscope operating at 200 kV and fitted with a Gatan Orius SC600A CCD camera to obtain the images of TEM, HRTEM, selected area electron diffraction (SAED) and the data of energy dispersive X-ray (TEM-EDX) analysis. During all analyses, the microscope was operated in a low dose mode and the sample exposure time was controlled to avoid beam damages on the observed particles. The cryo-TEM experiments were performed on a FEI Talos F200C which was equipped with a LaB6 filament operating at 200 kV and the images were recorded using a 4k × 4k Ceta CCD (charge-coupled device) camera. A Gatan cryo-holder operating at ~ -170 ^{o}C was used to hold the samples.

Results and discussion

Formation and aggregation of ACS nanoparticles

Upon mixing of the preheated Na_2SO_4 solution (90 ^{o}C) into the preheated concentrated $CaCl_2$ solution (90 ^{o}C), a chain of spheroidal nanoparticles with diameters of 20 – 50 nm were observed

in 1 min (Fig. 1a). The low-dose SAED pattern (Fig. 1a, inset) with diffuse rings indicated that the spheroidal nanoparticles were in the amorphous phase. The cryo-TEM analysis further identified that the spheroidal amorphous nanoparticles were not sample quenching artefacts, because the spheroidal amorphous nanoparticles with identical dimension and diffuse SAED pattern to that of the amorphous nanoparticles in Figure 1a were captured using the cryogenic quenching method (Fig. 1b). The Energy dispersive X-ray (EDX) analysis with obvious Ca, S and O signals showed that the amorphous nanoparticles were composed of $CaSO_4$, and no Na or Cl was detected, confirming that the sample quenching method worked well to achieve a quick solid-liquid separation and to acquire the ACS nanoparticles without $CaCl_2$ or Na_2SO_4 residuals (Fig. 2).

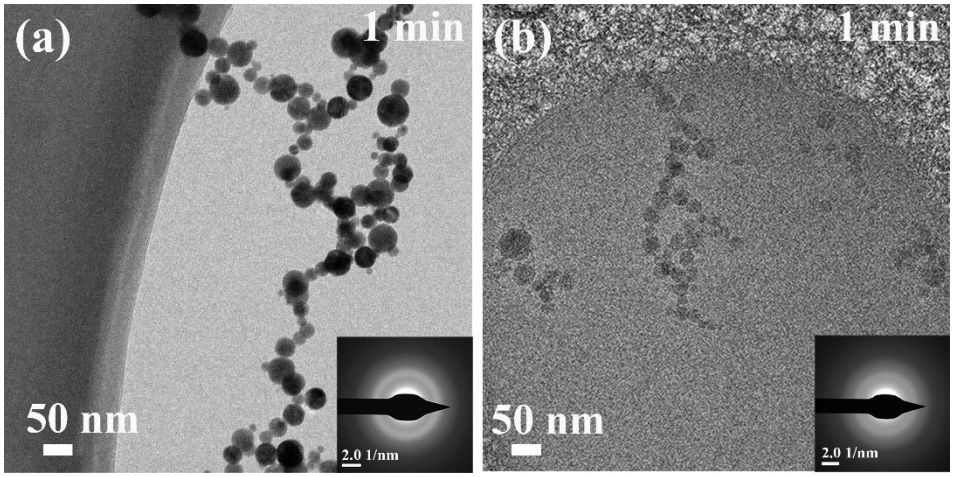

Fig. 1 Formation of ACS nanoparticles in 1 minute after the mixing of precursor solutions of $CaCl_2$ and Na_2SO_4. (a) TEM and (b) cryo-TEM images and low-dose SAED patterns (inset) of the spheroidal nanoparticles obtained by vacuum / solvent filtration and cryogenic quenching method respectively.

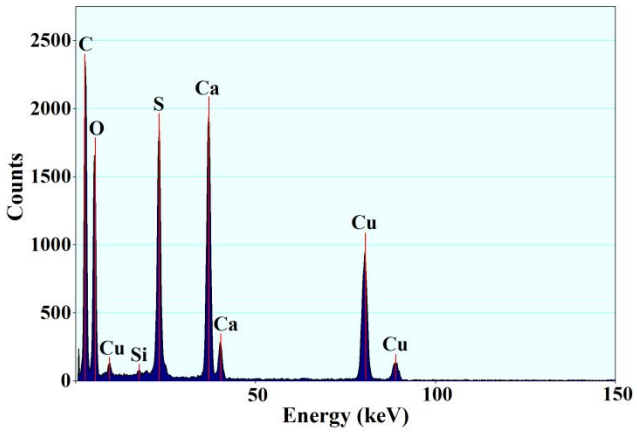

Fig. 2 TEM-EDX spectrum of the formed ACS nanoparticles. The strong Ca, S and O signals correspond to the composition of calcium sulfate. The C, Cu and Si signals stem from the carbon coated Cu-TEM grid and the sample holder.

The existence of ACS as a precursor to calcium sulfate crystallization has been in doubt for decades. Here we captured the ACS nanoparticles as a precursor to calcium sulfate crystallization in the condition of 4.00 mM $CaSO_4$ solution at 90 °C, which is supersaturated with respect to gypsum (saturation index SI_{Gyp} = + 1.013), bassanite (SI_{Bas} = + 1.254) and anhydrite (SI_{Anh} = + 1.610) (see Supporting Information for more detail). Moreover, the ACS nanoparticles were obtained in sufficient temporal and spatial resolution, and presented a distinct dimension and morphology.

The ACS nanoparticles were short-lived in solution and prone to aggregate into large ACS particles as shown by the ACS particles obtained at 10 min in Fig. 3a. The HRTEM image in Fig. 3c showed that the aggregated large ACS particles presented a compact morphology. After 20 min of reaction, the spheroidal ACS particles grew to a dimension of 80 – 150 nm (Fig. 3b). The low-dose SAED pattern (Fig. 3b, inset) and HRTEM image (Fig. 3d) showed that the growing

ACS particles maintained its amorphous character. This evolution infers that ACS may experience a series of amorphous states.

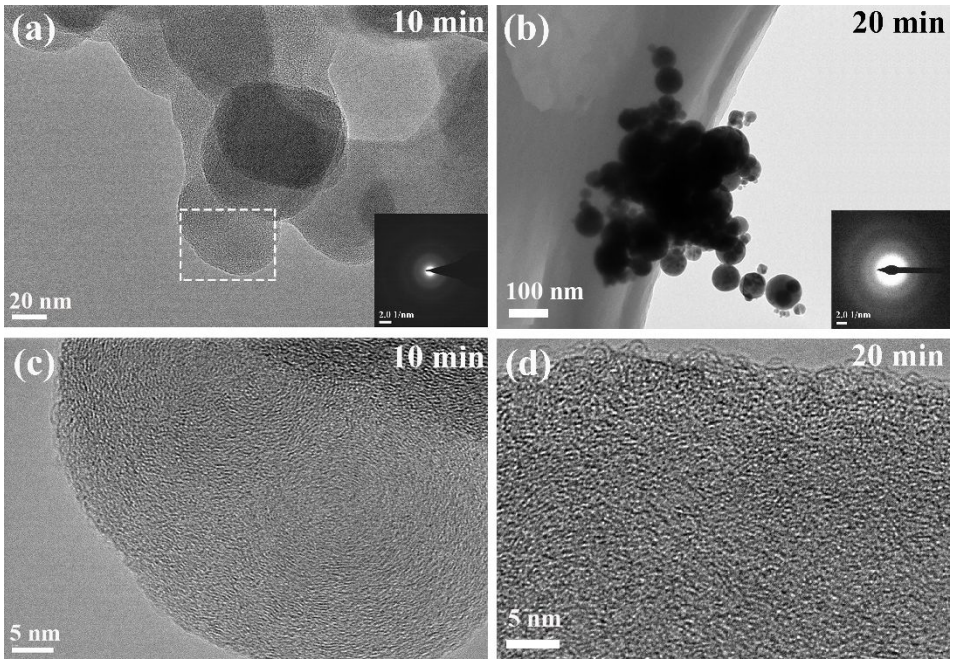

Fig. 3 Aggregation and growth of the ACS nanoparticles. (a, b) TEM images and low-dose SAED patterns (inset) of the ACS particles obtained at 10 min and 20 min. (c, d) HRTEM images of the amorphous (nano)particles in (a) and (b). The white square in (a) indexed to the area for HRTEM analysis.

Nanocrystalline domains development within bulk ACS

After the appearance of the more compact morphology, bulk ACS particles with irregular morphology were generated at 30 min, which coexisted with a population of spheroidal nanoparticles attached on the surface (Fig. 4a). SAED analysis showed that these attached nanoparticles were amorphous (Fig. S1), whereas some of the aggregates presented weak diffraction spots (Fig. 4b-1, 2) which indicated the onset of crystallization within the bulk ACS

particle (Fig. 4c). The formation of an arbitrary number of randomly distributed nanocrystalline domains with diameters of 2 - 5 nm as outlined by the white dashed circles in Fig. 4c revealed that the crystallization of ACS occurred randomly within the ACS particle. Further fusion and growth yielded a more compact structure (Fig. 4a, area 3) and a prevalent growth of nanocrystalline domains with multiple crystallographic orientations, which were confirmed by the concentric diffraction rings (Fig. 4b – 3, marked in blue) and the randomly oriented lattice fringes (Fig. 4d; Fig. S2) that were assigned to gypsum (PDF2 33-311).

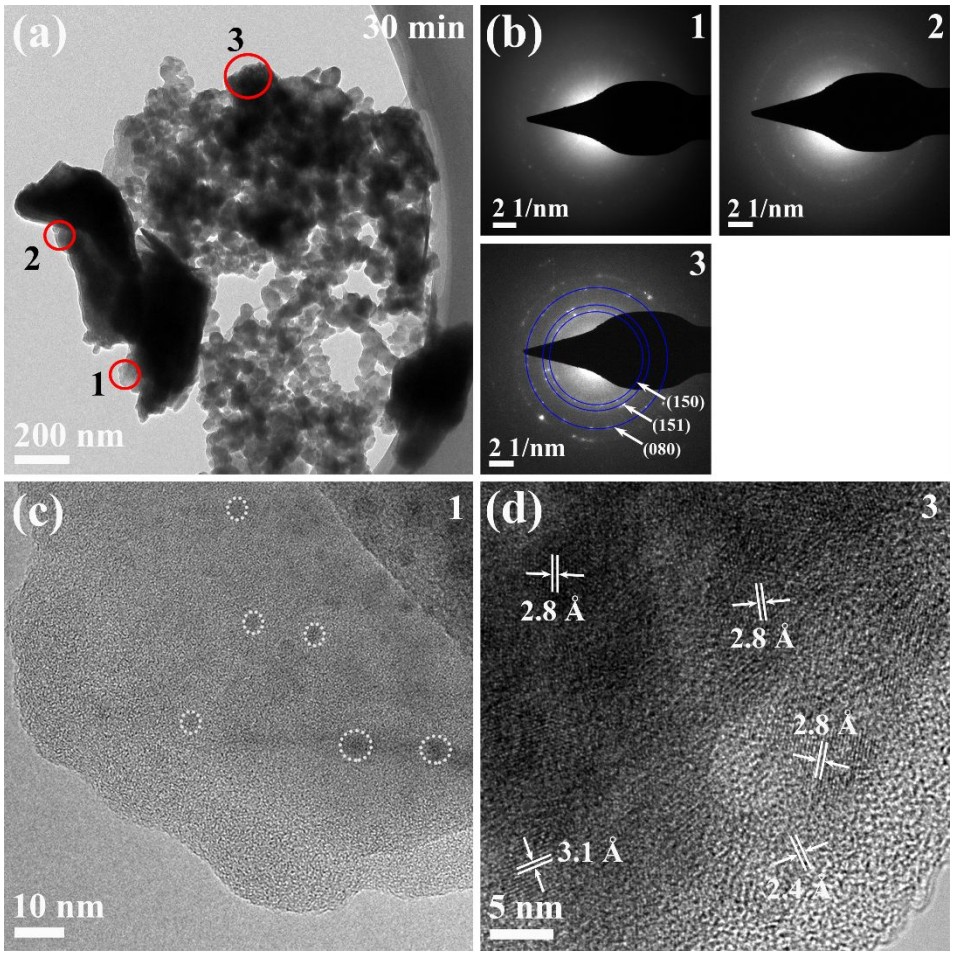

Fig. 4 Formation of nanocrystalline domains within the ACS particles. (a) Bulk ACS particles coexisting with individual ACS nanoparticles (30 min). (b) Diffraction patterns of the areas 1 - 3,

showing the development of crystallinity. The diffraction rings (marked in blue in b-3) index to the plane of (150), (151) and (080) of gypsum (PDF2 33-311). (c, d) HRTEM images of the areas 1 and 3 with marked lattice spacings corresponding to gypsum (3.1 Å, 2.8 Å and 2.4 Å). Several randomly distributed nanocrystalline domains were outlined by white dashed circles in (c).

Thereafter, micron-sized and well-faceted gypsum crystals were generated at 40 min with remnants of the aggregated particles attached on the surface (Fig. 5a); these particles may serve as the feedstock for gypsum crystal growth by a dissolution-reprecipitation mechanism.[34] The SAED pattern (Fig. 5a, inset) and HRTEM image (Fig. 5b) identified the concomitant growth and orientation of the crystalline domains within the ACS particles to form the monocrystalline gypsum domains with roughly identical orientations of lattice fringes. The monocrystalline gypsum domains grow by further addition of ions from solution or from the dissolution of the attached ACS nanoparticles on the surface.[34]

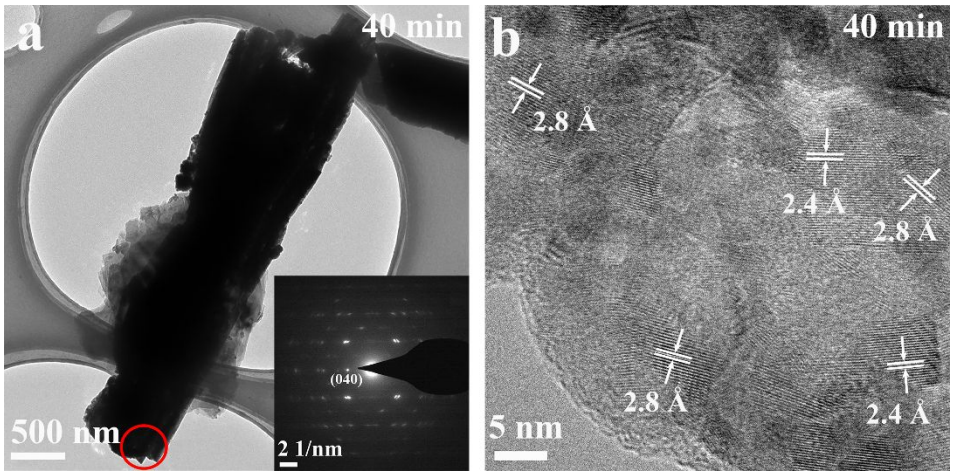

Fig. 5 Formation of crystalline gypsum phase. (a) Gypsum with aggregated particles attached on the surface (40 min). (b) HRTEM image of the area outlined by the red circle in (a) with marked

lattice spacings corresponding to gypsum (3.1 Å, 2.8 Å and 2.4 Å).

Mechanism of ACS Crystallization

This time-resolved observation showed that the ACS nanoparticles were precipitated from solution during the crystallization of calcium sulfate and transformed into the kinetically most accessible gypsum phase in the later stage. Previous studies have reported the similar crystallization pathway of calcium sulfate, which demonstrates that although anhydrite is the thermodynamically most stable phase at elevated temperatures in certain concentrated solutions, gypsum is nucleated prior to anhydrite.[35-37]

Moreover, this work makes a clear profile for the structural development of the aggregation-based transformation of the ACS nanoparticles into the crystalline gypsum phase. Aggregation and fusion of the ACS nanoparticles may derive from the development of short-range to medium-range order of the growing ACS particles. Development of the lattice structure and the multiple nanocrystalline domains inside the ACS material suggest a seemingly solution-like character of the amorphous material that allows for lattice ions transport from one domain to the other and thus facilitates numerous isolated nucleation events to take place. The growth of nanocrystalline domains and the internal structural orientation to yield monocrystalline gypsum domains require the reorganization of lattice ions and therefore the mass transport within the ACS material.[38, 39]

Based on the experimental observations, we outline five distinct stages of the evolution of ACS nanoparticles into the crystalline gypsum phase as shown in Fig.6. The first stage is the

formation of spheroidal ACS nanoparticles in a highly disordered structure (stage 1). The ACS nanoparticles grow into larger particles and the simultaneous fusion and internal structural evolution generate a compact morphology (stage 2 and 3). Aggregation of the ACS particles initiates the growth of the bulk ACS particle, and then nanocrystalline domains with multiple crystallographic orientations are formed randomly inside the bulk ACS particle (stage 4). Growth and orientation of the nanocrystalline domains generate the monocrystalline gypsum domains that evolve from polycrystal to monocrystal (stage 5). Further growth of the monocrystalline gypsum domains by ions addition from solution or from the dissolution of the attached ACS nanoparticles generates the micron-sized gypsum crystals (stage 6).

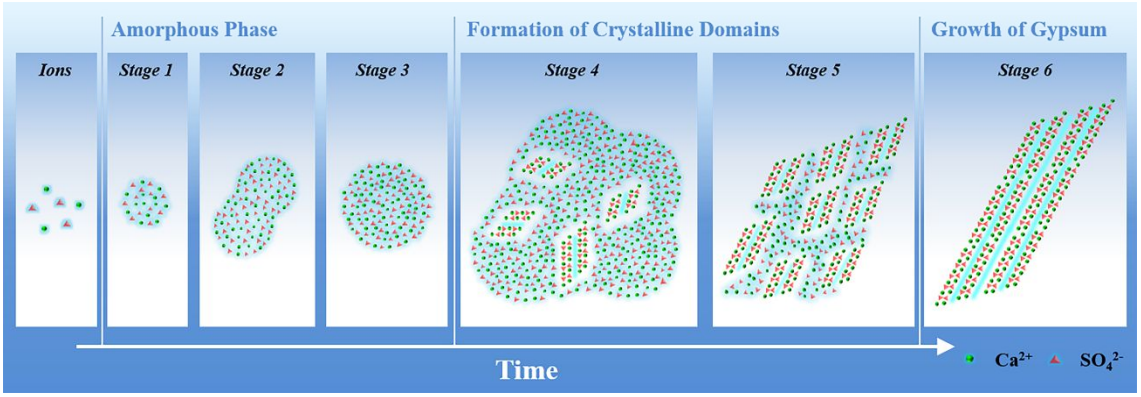

Fig.6 Schematic illustration of the evolution of the ACS nanoparticles to the crystalline gypsum phase. Stage 1: formation of ACS nanoparticles. Stage 2: aggregation and fusion of the ACS nanoparticles. Stage 3: growth of the fused ACS nanoparticles to form the ACS particles. Stage 4: random formation of nanocrystalline domains inside the bulk ACS particle. Stage 5: prevalent growth and orientation of the crystalline gypsum domains. Stage 6: growth of the micron-sized gypsum crystals by ions addition.

Conclusions

The crystallization of calcium sulfate begins with the formation of ACS nanoparticles that present a spectrum of morphologies developing from a relatively loose form to a compact one. Aggregation of the ACS nanoparticles forms the bulk ACS particle within which separate nanocrystalline domains develop and evolve from multiple crystallographic orientations to the monocrystalline gypsum domains. This study characterizes several stages of the structural evolution within the amorphous precursors that provides an insight into the evolution of the ACS precursor into the crystalline gypsum phase that appears central to the understanding of multistage crystallization in natural environments and in industrial applications.

Acknowledgements

Financial support is provided by the National Key Research and Development Program of China (Grants 2019YFC0408802) and National Natural Science Foundation of China (Project 21176219). We thank Shenghai Chang in the Center of Cryo-Electron Microscopy (CCEM), Zhejiang University for his technical assistance on Cryo-Transmission Electron Microscopy. Great thanks to Sebastian T. Mergelsberg who helped calculate the supersaturation index of the calcium sulfate phases. Special thanks to Dr. Savero Keith who has contributed to the organization of the paper.

References

1. J. Rieger, M. Kellermeier and L. Nicoleau, *Angew. Chem. Int. Ed.*, 2014, **53**, 12380-12396.

2. J. J. De Yoreo, P. U. P. A. Gilbert, N. A. J. M. Sommerdijk, R. L. Penn, S. Whitelam, D. Joester, H. Zhang, J. D. Rimer, A. Navrotsky, J. F. Banfield, A. F. Wallace, F. M. Michel, F. C. Meldrum, H. Colfen and P. M. Dove, *Science*, 2015, **349**, a6760.

3. M. A. Boles, M. Engel and D. V. Talapin, *Chem. Rev.*, 2016, **116**, 11220-11289.

4. L. B. Gower, *Chem. Rev.*, 2008, **108**, 4551-4627.

5. W. Sun, S. Jayaraman, W. Chen, K. A. Persson and G. Ceder, *Proc. Natl. Acad. Sci.*, 2015, **112**, 3199-3204.

6. Z. Lu and Y. Yin, *Chem. Soc. Rev.*, 2012, **41**, 6874-6887.

7. R. Sun, T. Willhammar, E. Svensson Grape, M. Strømme and O. Cheung, *Cryst. Growth Des.*, 2019, **19**, 5075-5087.

8. R. Sun, P. Zhang, É. G. Bajnóczi, A. Neagu, C. Tai, I. Persson, M. Strømme and O. Cheung, *ACS Appl. Mater. Inter.*, 2018, **10**, 21556-21564.

9. L. Addadi, S. Raz and S. Weiner, *Adv. Mater.*, 2003, **15**, 959-970.

10. T. H. Zhang and X. Y. Liu, *J. Am. Chem. Soc.*, 2007, **129**, 13520-13526.

11. G. Zhu, S. Yao, H. Zhai, Z. Liu, Y. Li, H. Pan and R. Tang, *Langmuir*, 2016, **32**, 8999-9004.

12. V. Uskokovic, S. Markovic, L. Veselinovic, S. Skapin, N. Ignjatovic and D. P. Uskokovic, *Phys. Chem. Chem. Phys.*, 2018, **20**, 29221-29235.

13. A. Dey, P. H. H. Bomans, F. A. Müller, J. Will, P. M. Frederik, G. de With and N. A. J. M. Sommerdijk, *Nat. Mater.*, 2010, **9**, 1010-1014.

14. B. P. Pichon, P. H. H. Bomans, P. M. Frederik and N. A. J. M. Sommerdijk, *J. Am. Chem. Soc.*, 2008, **130**, 4034-4040.

15. J. D. Rodriguez-Blanco, S. Shaw and L. G. Benning, *Nanoscale*, 2011, **3**, 265-271.

16. S. Sun, D. Gebauer and H. C Lfen, *Angew. Chem. Int. Ed.*, 2017, **56**, 4042-4046.

17. D. A. M. J. Joanna Aizenberg and D. R. Hamann, *Science*, 2003, **299**, 1205-1208.

18. J. De Yoreo, *Nat. Mater.*, 2013, **12**, 284-285.

19. H. Tong, W. Ma, L. Wang, P. Wan, J. Hu and L. Cao, *Biomaterials*, 2004, **25**, 3923-3929.

20. D. Freyer and W. Voigt, *Monatshefte für Chemie / Chemical Monthly*, 2003, **134**, 693-719.

21. F. Otàlora and J. M. García-Ruiz, *Chem. Soc. Rev.*, 2014, **43**, 2013-2026.

22. Q. Chen, C. Jia, Y. Li, J. Xu, B. Guan and M. Z. Yates, *Langmuir*, 2017, **33**, 2362-2369.

23. A. E. S. Van Driessche, L. G. Benning, J. D. Rodriguez-Blanco, M. Ossorio, P. Bots and J. M. García-Ruiz, *Science*, 2012, **336**, 69-72.

24. T. M. Stawski, A. E. S. van Driessche, M. Ossorio, J. Diego Rodriguez-Blanco, R. Besselink and L. G. Benning, *Nat. Commun.*, 2016, **7**, 11177.

25. P. Tartaj, J. Morales and L. Fernández-Díaz, *Cryst. Growth Des.*, 2015, **15**, 2809-2816.

26. C. Jia, Q. Chen, X. Zhou, H. Wang, G. Jiang and B. Guan, *Ind. Eng. Chem. Res.*, 2016, **55**, 9189-9194.

27. Y. Wang, Y. Kim, H. K. Christenson and F. C. Meldrum, *Chem. Commun.*, 2012, **48**, 504-506.

28. A. Saha, J. Lee, S. M. Pancera, M. F. Bräeu, A. Kempter, A. Tripathi and A. Bose, *Langmuir*,

2012, **28**, 11182-11187.

29. F. Jones, *CrystEngComm*, 2012, **14**, 8374-8381.

30. Z. Zou, W. J. E. M. Habraken, G. Matveeva, A. C. S. Jensen, L. Bertinetti, M. A. Hood, C. Sun, P. U. P. A. Gilbert, I. Polishchuk, B. Pokroy, J. Mahamid, Y. Politi, S. Weiner, P. Werner, S. Bette, R. Dinnebier, U. Kolb, E. Zolotoyabko and P. Fratzl, *Science*, 2019, **363**, 396-400.

31. E. M. Pouget, P. H. H. Bomans, J. A. C. M. Goos, P. M. Frederik, G. De With and N. A. J. M. Sommerdijk, *Science*, 2009, **323**, 1455-1458.

32. J. Baumgartner, A. Dey, P. H. H. Bomans, C. Le Coadou, P. Fratzl, N. A. J. M. Sommerdijk and D. Faivre, *Nat. Mater.*, 2013, **12**, 310-314.

33. W. J. E. M. Habraken, J. Tao, L. J. Brylka, H. Friedrich, L. Bertinetti, A. S. Schenk, A. Verch, V. Dmitrovic, P. H. H. Bomans, P. M. Frederik, J. Laven, P. van der Schoot, B. Aichmayer, G. de With, J. J. DeYoreo and N. A. J. M. Sommerdijk, *Nat. Commun.*, 2013, **4**, 1507.

34. C. Rodriguez-Navarro, A. Burgos Cara, K. Elert, C. V. Putnis and E. Ruiz-Agudo, *Cryst. Growth Des.*, 2016, **16**, 1850-1860.

35. S. He, J. E. Oddo and M. B. Tomson, *J. Colloid Interf. Sci.*, 1994, **162**, 297-303.

36. Z. Li and G. P. Demopoulos, *Ind. Eng. Chem. Res.*, 2006, **45**, 4517-4524.

37. H. Fu, B. Guan, G. Jiang, M. Z. Yates and Z. Wu, *Cryst. Growth Des.*, 2012, **12**, 1388-1394.

38. E. M. Pouget, P. H. H. Bomans, A. Dey, P. M. Frederik, G. de With and N. A. J. M. Sommerdijk, *J. Am. Chem. Soc.*, 2010, **132**, 11560-11565.

39. Q. Chen, L. Wu, Y. Zeng, C. Jia, J. Lin, M. Z. Yates and B. Guan, *CrystEngComm*, 2019, **21**, 5973-5979.

Table of Contents

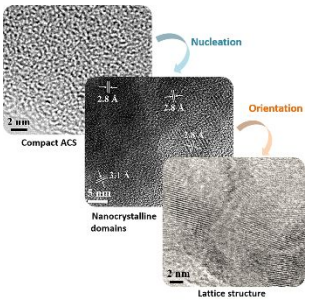

Growth and orientation of the nanocrystalline domains within the fused ACS particles generates the monocrystalline gypsum phase.